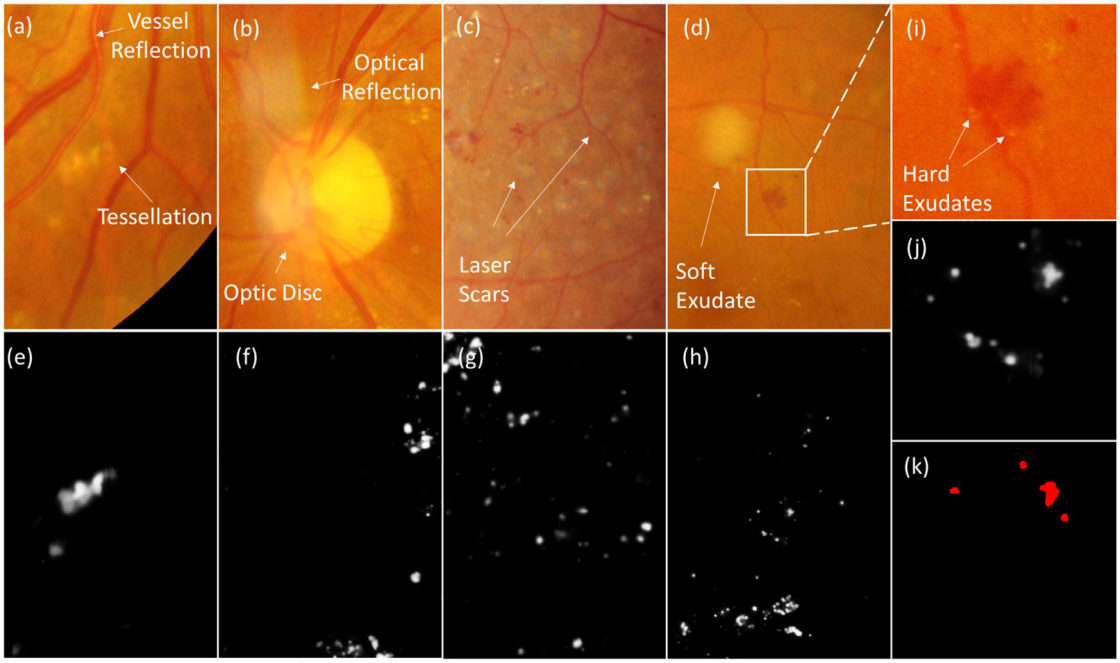

Fig. 11. Illustration of (a-d) different challenging circumstances for segmentation of EXs, (e-h) segmentation results (probability map) of the top-performing team for EXs, (i) enlarged part of Fig. (d), and (j) depicts its performance to be better than (k) the human annotator (The annotator tool had a limitation of the markup capability when there is an overlap of multiple types of lesion. In this case, EXs and HE).

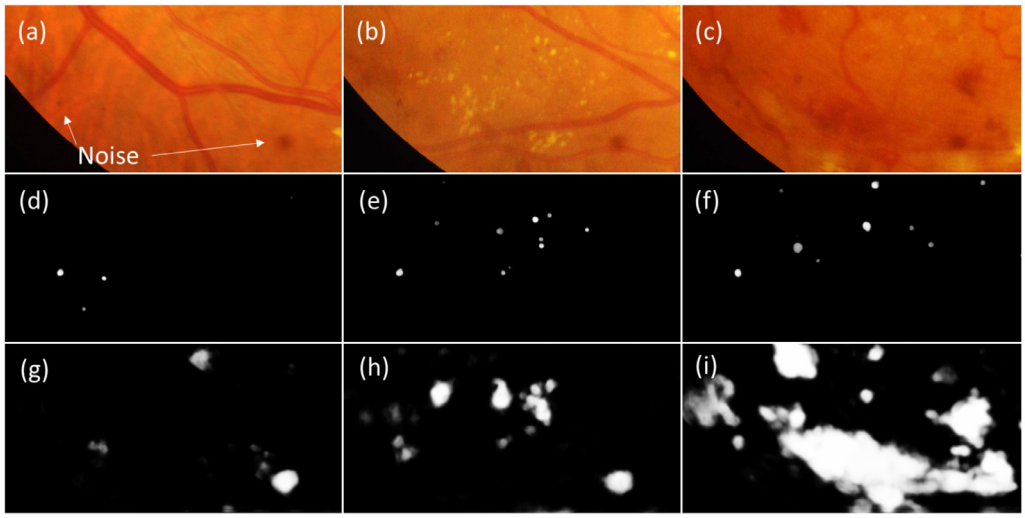

Fig. 12. Illustration of results by top performing solutions for (a-c) different images with noise causing most common false positives in the segmentation of (d-f) MAs, and (g-i) HEs respectively.

0.6311 as shown in Table 9. Notably, all teams except AVASAVA used the external Kaggle DR dataset for pre-training their models. This dataset contains a large number of retina images annotated with the disease level, in contrast, team AVASAVA pre-trained their model on ImageNet, a dataset containing natural images and object annotations, effectively showing the network a much smaller number of retina images at the training stage, approximately 1% compared to the other teams. This indicates that in the presence of a limited number of labeled data, transfer learning approaches along with the good model pruning could yield comparable and competitive results. However, while the models do determine the variability of performance, the number, type, and quality of training data is a crucial factor for a fair comparison of competing solutions. There is still work needed on simultaneous grading of DR and DME as the reported results do not yet reach the performance needed for a clinically viable automatic screening. Considering the misclassified instances in confusion matrices shown in Table 12, along with the lesion information, it is essential to give attention towards characterization of intra-retinal microvascular abnormalities (IRMA's) and venous beading for improvement in the overall grading results.

In the sub-challenge – 3, another on-site challenge, four teams were evaluated for the task of OD/fovea localization and OD segmentation. For the task of OD localization, the Euclidean distance varied between 21.072 and 36.22 (lower values indicate better performance). However, for Fovea localization task the same performance metric ranged between 64.492 and 570.133. This massive variation is due to outliers, e.g. team ZJU-BII-SGEX had 23 outliers

Table 12
Confusion matrix of retinal images predicted by top performing solution for DR (5 class) and DME (3 class).

Actual \ Predicted	0	1	2	3	4
0	**30**	0	2	1	1
1	3	**1**	1	0	0
2	3	2	**22**	4	1
3	2	0	1	**13**	3
4	1	0	1	0	**11**

Actual \ Predicted	0	1	2
0	**40**	2	3
1	5	**2**	3
2	5	2	**41**

whose Euclidean distance exceeded 700. In the OD segmentation task, the average Jaccard similarity index score amongst the participants ranged between 0.7892 and 0.9338. The top-performing solutions developed by DeepDR and VRT leveraged prior clinical knowledge, such as the number of landmarks and their geometric relationship to detect another retinal landmark. It is also observed that data augmentation and ensemble of models yield substantial improvements in terms of accuracy. Considering the clinical significance of OD diameter while DME severity grading, we further compute the average OD diameter (in pixels) for each image of the test set. The average diameter of OD ground truth is 516.61 pixels, whereas, corresponding values for the results of solutions developed by the teams ZJU-BII-SGEX, VRT, IITKgpKLIV, CBER and SDNU are 514.25, 519.21, 513.48, 508.04 and 460.19 pixels respectively. Team CBER submitted their results after the competition and they were not included in the leaderboard.

As expected, we found that image resolution is a vital factor for the model performance, especially for the task of segmentation of small objects such as MAs or EXs. In fact, the top-performing approaches processed the images patch-wise, which allow models to have a local high-resolution image view or directly with the high-resolution image as a whole. This is essential as MAs or small EXs lesions span very few pixels in some cases, and reducing the original image size would prevent an accurate segmentation. Similarly, image resolution plays a very important role for disease classification task (see Table 9), the most likely reason is that presence of the disease is determined by the presence of lesions in the image, including the small ones that might be invisible at low resolution. This is corroborated by the confusion matrices in Table 12 which show misclassified instances in DR (particularly, grade 1 and 2) as well as DME (5 images each belonging to grade 1 and 2 are predicted as grade 0). For the localization tasks, all participants were asked to identify retinal structures with coordinates at full image resolution. Most of them performed these tasks by scaling image to the smaller size and then converted their predictions in the original image space. Comparative analysis indicates that the input image resolution has limited effect on the results of the localization problem. For instance, in the case of OD localization, the top-performing team utilized two image resolutions, one (224×224 pixels) for approximate location prediction and other (cropped ROIs 950×950 pixels) for refining that estimate. Similarly, teams CBER and VRT resized the image to 536×356 pixels and 640×640 pixels respectively to get an approximate center location whereas the team SDNU utilized the input size of 1984×1318 pixels. Considering the OD average diameter of approximately 516 pixels, limited performance variation (10 to 15 pixels) is observed as compared to the top-performing solution for huge variation (multiple times) in input resolutions (see Table 10). This is because the retinal structures to be identified, OD and fovea, are very unlikely to disappear due to a reduction of image resolution and they have clear geometrical constraints.

As confirmed by recent studies (Krause et al., 2018; Son et al., 2019), we hypothesized that algorithms developed using images with fine visibility and images having high resolution with adjudicated consensus grades yield better performance when compared to datasets consisting of poor-quality (non-gradable) images and images captured in varied acquisition settings. Therefore, this challenge provides data collected in the routine clinical practice using an acquisition protocol consistent for all images. The data was acquired after pupil dilation with the same camera at the same resolution, ensuring consistent quality. This dataset did not include non-gradable images and images with substantial disagreement amongst the expert annotators. Even after these efforts to provide the best possible data, the annotation process is still inherently subjective, and the annotator judgment is a limiting factor for the method performance which is mostly trained and evaluated in a supervised manner. We also note that images captured with different retinal cameras or with different diseases would have allowed for a better estimation of the generalization ability of the proposed methods since they might be more representative from clinical settings. Further, while we believe that data challenges like ours foster "methodology diversity", the majority of competing solutions used deep convolutional networks. These approaches are comparably easier to implement than approaches based on feature engineering and do generalize well to multiple medical imaging domains, which in turn, dramatically reduces the need for specialized task knowledge. Notably, amongst the competing solutions in this challenge that utilized the deep learning approach along with the task-relevant subject knowledge have demonstrated superior performance. However, it seems there might be some impact of challenge duration, apart from the number of submissions, on the quality of developed solutions. Considering the time span from data availability to deadline of results submission, about one and a half month, was considerably tight for managing all tasks at the same time. For the team VRT who had been working on analyzing fundus images for more than a year when participated in the competition that attempting all tasks were possible, still, it was challenging for them to commit all the tasks. However, it would be highly challenging for a newcomer to succeed in multiple tasks. In that sense, the competition period was not sufficient for perfecting all tasks. However, it would be enough for a competent participant, e.g. new entrants in the field as team SAIHST, to finish one task if the participant can focus on the competition completely. Also, in this challenge, the results were evaluated all at once after the result submission deadline. However, a continuous on-line assessment of participating solutions would have facilitated the submission procedure by providing real-time feedback to the teams performance. This would have enabled a maximum number of submissions during the challenge period, probably boosting the final count of submissions. However, this would have introduced a risk of overfitting the test data by continuous submissions based on the system's performance on the test set.

This challenge led to the development of a variety of new robust solutions for lesion segmentation, detection, and segmentation of retinal landmarks and disease severity grading. Despite the complexity of the tasks, less than one-and-a-half month time for development, it received a very positive response, and the top-performing solutions were able to achieve results close to the human annotators. Still, there is room for improvement, especially in the lesion segmentation and disease-grading tasks. Though the competition is now completed, the dataset has been made publicly available for research purposes to attract newcomers to the problem and to encourage the development of novel solutions to meet current and future clinical standards.

Declaration of Competing Interest

The authors have no conflicts of interest to declare.

Table A.1
Summary of technical specifications and hardware used in different databases.

Name of Database	Number of Images	Technical Details				
		Image Size(s)	FOV	Camera	NMY	Format
ARIA	212	768 × 576	50	Zeiss *FF*450+	✓	TIFF
DIARETDB	130+89	1500 × 1152	50	Zeiss *FF*450+	✓	PNG
DRIVE	40	768 × 584	45	Canon *CR*5	✓	JPEG
E-Ophtha	47EX+35H 148MA+233H	1440 × 960 - 2048 × 1360 (4)	45	Canon *CR* – *DGI* & Topcon *TRC* – *NW*6	✓	JPEG
HEIMED	169	2196 × 1958	45	Zeiss Visucam PRO	✓	JPEG
Kaggle	88,702	433 × 289 - 3888 × 2592	Varying	Any camera (EyePACS Platform)	–	TIFF
MESSIDOR	800 MY+ 400 NMY+ 1756	1440 × 960, 2240 × 1488, 2304 × 1536	45	3CCD/ Topcon TRC NW6	Both	TIFF
ROC	100	768 × 576, 1058 × 1061, 1389 × 1383	45	Topcon *NW*100 & *NW*200 Canon *CR*5 – 45*NM*	✓	JPEG
STARE	397	605 × 700	35	Topcon *TRV* – 50	×	PPM
IDRiD	516 (81 with LA)	4288 × 2848	50	Kowa *VX* – 10α	✓	JPG

EX - Hard Exudate, MA - Microaneurysms, H - Healthy, MY - Mydriatic, NMY - Non-Mydriatic, FOV - Field of View, LA - Lesion Annotation.

Table A.2
Comparison of different databases with the IDRiD database.

Name of database	Normal fundus structures			Abnormalities				Multiple experts		DR grading	DME grading
	OD	VS	FA	MA	HE	EX	SE	Yes/No	#		
ARIA	✓	✓	✓	×	×	×	×	✓	2	×	×
DIARETDB1	×	×	×	✓	✓	✓	✓	✓	4	×	×
DRIVE	×	✓	×	×	×	×	×	✓	3	×	×
E-Optha	×	×	×	✓	×	✓	×	✓	2	×	×
HEIMED	×	×	×	×	×	✓	✓	×	1	×	✓
Kaggle	×	×	×	×	×	×	×	✓	2	✓	×
MESSIDOR	×	×	×	×	×	×	×	×	1	✓	✓
ROC	×	×	×	✓	×	×	×	✓	4	×	×
STARE	✓	✓	×	×	×	×	×	✓	2	×	×
IDRiD	✓	×	✓	✓	✓	✓	✓	✓	2	✓	✓

OD - Optic Disc, VS - Vessels, FA - Fovea, MA - Microaneurysms, HE - Hemorrhage, EX - Hard Exudate, SE - Soft Exudate, # - Number of Experts

Acknowledgments

This work is sponsored by the Shri Guru Gobind Singhji Institute of Engineering and Technology, Nanded (M.S.), INDIA. The authors would like to thank the following people for their help in various aspects of organizing the ISBI-2018 Diabetic Retinopathy Segmentation and Grading Challenge: Prof. Emanuele Trucco (University of Dundee, Scotland), Tom MacGillivray (University of Edinburgh, Scotland), Ravi Kamble (SGGS Institute of Engineering and Technology, Nanded), Prof. Vivek Sahasrabuddhe (Government Medical College, Nanded) and Désiré Sidibé (Université de Bourgogne, France). We would also like to thank Prof. Jorge Cuadros, University of California, Berkeley (Organizer of Kaggle Diabetic Retinopathy challenge) for his kind permission for reporting the results of the models trained on their dataset. *VRT*: This study was supported by the Research Grant for Intelligence Information Service Expansion Project, which is funded by.National IT Industry Promotion Agency (NIPA-C0202-17-1045) in South Korea. *DeepDR*: This work was supported in part by the National Natural Science Foundation of China under Grant Grant 61872241, Grant 61572316, in part by the National Key Research and Development Program of China under Grant 2016YFC1300302 and Grant 2017YFE0104000, in part by the Science and Technology Commission of Shanghai Municipality under Grant 16DZ0501100 and Grant 17411952600. *HarangiM1-M2*: Research was supported in part by the Janos Bolyai Research Scholarship of the Hungarian Academy of Sciences and the project EFOP-3.6.2-16-2017-00015 supported by the European Union and the State of Hungary, co-financed by the European Social Fund. *ZJU-BII-SGEX*: This work is supported by Beijing Shanggong Medical Technology Co., Ltd., which provided ocular healthcare solutions in China. This research is partially supported by the A*STAR A1818g0022 grant of Singapore. Many thanks to the labeled images from Image Annotation Group of Beijing Shanggong Medical Technology. Team *CBER* (A.M. Mendonça, T. Melo, T. Araújo and A. Campilho) is financed by the ERDF European Regional Development Fund through the Operational Programme for Competitiveness and Internationalisation - COMPETE 2020 Programme, and by National Funds through the FCT Fundação para a Ciência e a Tecnologia (Portuguese Foundation for Science and Technology) within project CMUP-ERI/TIC/0028/2014. Teresa Araújo is funded by the FCT grant SFRH/BD/122365/2016. *SDNU:* This study was supported by the National Natural Science Foundation of China (Grant No. 61572300).

Appendix A. Comparison of Publicly Available Retinal Image Databases

Table A.1 and Table A.2 provides the summary of technical specifications and available ground truths in several existing datasets and the IDRiD dataset.

Supplementary material

Supplementary material associated with this article can be found, in the online version, at doi:10.1016/j.media.2019.101561

References

Abdulla, W., 2017. Mask r-CNN for object detection and instance segmentation on keras and tensorflow. https://github.com/matterport/Mask_RCNN.

Abràmoff, M.D., Garvin, M.K., Sonka, M., 2010. Retinal imaging and image analysis. IEEE Rev. Biomed. Eng. 3, 169–208.

Abràmoff, M.D., Lou, Y., Erginay, A., Clarida, W., Amelon, R., Folk, J.C., Niemeijer, M., 2016. Improved automated detection of diabetic retinopathy on a publicly available dataset through integration of deep learning. Investigat. Ophthalmol. Vis. Sci. 57 (13), 5200–5206.

Acharya, R., Chua, C.K., Ng, E., Yu, W., Chee, C., 2008. Application of higher order spectra for the identification of diabetes retinopathy stages. J. Med. Syst. 32 (6), 481–488.

Acharya, U.R., Mookiah, M.R.K., Koh, J.E.W., Tan, J.H., Bhandary, S.V., Rao, A.K., Hagiwara, Y., Chua, C.K., Laude, A., 2017. Automated diabetic macular edema (DME) grading system using DWT, DCT features and maculopathy index. Comput. Biol. Med. 84, 59–68.

Acharya, U.R., Ng, E.Y.-K., Tan, J.-H., Sree, S.V., Ng, K.-H., 2012. An integrated index for the identification of diabetic retinopathy stages using texture parameters. J. Med. Syst. 36 (3), 2011–2020.

Adal, K.M., Sidibé, D., Ali, S., Chaum, E., Karnowski, T.P., Mériaudeau, F., 2014. Automated detection of microaneurysms using scale-adapted blob analysis and semi-supervised learning. Comput. Method. Progr.. Biomed. 114 (1), 1–10.

Agurto, C., Murray, V., Barriga, E., Murillo, S., Pattichis, M., Davis, H., Russell, S., Abràmoff, M., Soliz, P., 2010. Multiscale AM-FM methods for diabetic retinopathy lesion detection. IEEE Trans. Med. Imag. 29 (2), 502–512.

Almazroa, A., Alodhayb, S., Osman, E., Ramadan, E., Hummadi, M., Dlaim, M., Alkatee, M., Raahemifar, K., Lakshminarayanan, V., 2018. Retinal fundus images for glaucoma analysis: the RIGA dataset. In: Medical Imaging 2018: Imaging Informatics for Healthcare, Research, and Applications, Vol. 10579. International Society for Optics and Photonics, p. 105790B.

Antal, B., Hajdu, A., 2012. Improving microaneurysm detection using an optimally selected subset of candidate extractors and preprocessing methods. Pattern Recognit. 45 (1), 264–270.

Antal, B., Hajdu, A., 2014. An ensemble-based system for automatic screening of diabetic retinopathy. Knowl.-Based Syst. 60, 20–27.

Atlas, I.D.F.D., 2017. Brussels, belgium: international diabetes federation. Int. Diabet. Federat. (IDF). http://diabetesatlas.org/resources/2017-atlas.html

Badrinarayanan, V., Kendall, A., Cipolla, R., 2015. Segnet: a deep convolutional encoder-decoder architecture for image segmentation. arXiv preprint arXiv:1511.00561.

Bai, J., Miri, M.S., Liu, Y., Saha, P., Garvin, M., Wu, X., 2014. Graph-based optimal multi-surface segmentation with a star-shaped prior: application to the segmentation of the optic disc and cup. In: 2014 IEEE 11th International Symposium on Biomedical Imaging (ISBI). IEEE, pp. 525–528.

Bandello, F., Parodi, M.B., Lanzetta, P., Loewenstein, A., Massin, P., Menchini, F., Veritti, D., 2010. Diabetic macular edema. In: Macular Edema, Vol. 47. Karger Publishers, pp. 73–110.

Biyani, R.S., Patre, B.M., 2018. Algorithms for red lesion detection in diabetic retinopathy: a review. Biomed. Pharmacother. 107, 681–688.

Bourne, R.R.A., Stevens, G.A., White, R.A., Smith, J.L., Flaxman, S.R., Price, H., Jonas, J.B., Keeffe, J., Leasher, J., Naidoo, K., et al., 2013. Causes of vision loss worldwide, 1990–2010: a systematic analysis. Lancet Global Health 1 (6), e339–e349.

Boyd, K., Eng, K.H., Page, C.D., 2013. Area under the precision-recall curve: point estimates and confidence intervals. In: Joint European Conference on Machine Learning and Knowledge Discovery in Databases. Springer, pp. 451–466.

Carin, L., Pencina, M.J., 2018. On deep learning for medical image analysis. JAMA 320 (11), 1192–1193.

Carmona, E.J., Rincón, M., García-Feijoó, J., Martínez-de-la Casa, J.M., 2008. Identification of the optic nerve head with genetic algorithms. Artif. Intell. Med. 43 (3), 243–259.

Carson Lam, D.Y., Guo, M., Lindsey, T., 2018. Automated detection of diabetic retinopathy using deep learning. AMIA Summit. Translat. Sci. Proc. 2017, 147.

Cheng, J., Yin, F., Wong, D.W.K., Tao, D., Liu, J., 2015. Sparse dissimilarity-constrained coding for glaucoma screening. IEEE Trans. Biomed. Eng. 62 (5), 1395–1403.

Ching, T., Himmelstein, D.S., Beaulieu-Jones, B.K., Kalinin, A.A., Do, B.T., Way, G.P., Ferrero, E., Agapow, P.-M., Zietz, M., Hoffman, M.M., et al., 2018. Opportunities and obstacles for deep learning in biology and medicine. J. R. Soc. Interface 15 (141), 20170387.

Chudzik, P., Majumdar, S., Calivá, F., Al-Diri, B., Hunter, A., 2018. Microaneurysm detection using fully convolutional neural networks. Comput. Method. Progr. Biomed. 158, 185–192.

Ciulla, T.A., Amador, A.G., Zinman, B., 2003. Diabetic retinopathy and diabetic macular edema: pathophysiology, screening, and novel therapies. Diabetes Care 26 (9), 2653–2664.

Cuadros, J., Bresnick, G., 2009. EyePACS: an adaptable telemedicine system for diabetic retinopathy screening. J. Diabetes Sci. Technol. 3 (3), 509–516.

Dai, L., Fang, R., Li, H., Hou, X., Sheng, B., Wu, Q., Jia, W., 2018. Clinical report guided retinal microaneurysm detection with multi-sieving deep learning. IEEE Trans. Med. Imag. 37 (5), 1149–1161.

Das, V., Puhan, N.B., Panda, R., 2015. Entropy thresholding based microaneurysm detection in fundus images. In: 2015 Fifth National Conference on Computer Vision, Pattern Recognition, Image Processing and Graphics (NCVPRIPG). IEEE, pp. 1–4.

Dashtbozorg, B., Mendonça, A.M., Campilho, A., 2015. Optic disc segmentation using the sliding band filter. Comput. Biol. Med. 56, 1–12.

Decencière, E., Cazuguel, G., Zhang, X., Thibault, G., Klein, J.-C., Meyer, F., Marcotegui, B., Quellec, G., Lamard, M., Danno, R., et al., 2013. Teleophta: machine learning and image processing methods for teleophthalmology. IRBM 34 (2), 196–203.

Decencière, E., Zhang, X., Cazuguel, G., Laÿ, B., Cochener, B., Trone, C., Gain, P., Ordóñez Varela, J.-R., Massin, P., Erginay, A., et al., 2014. Feedback on a publicly distributed image database: the messidor database. Image Anal. Stereol. 33 (3), 231–234.

Deepak, K.S., Sivaswamy, J., 2012. Automatic assessment of macular edema from color retinal images. IEEE Trans. Med. Imag. 31 (3), 766–776.

Dhara, A.K., Mukhopadhyay, S., Bency, M.J., Rangayyan, R.M., Bansal, R., Gupta, A., 2015. Development of a screening tool for staging of diabetic retinopathy in fundus images. In: Medical Imaging 2015: Computer-Aided Diagnosis, Vol. 9414. International Society for Optics and Photonics, p. 94140H.

Dobbin, K.K., Simon, R.M., 2011. Optimally splitting cases for training and testing high dimensional classifiers. BMC Med. Genom. 4 (1), 31.

Esteves, T., Quelhas, P., Mendonça, A.M., Campilho, A., 2012. Gradient convergence filters and a phase congruency approach for in vivo cell nuclei detection. Mach. Vis. Appl. 23 (4), 623–638.

Everingham, M., Van Gool, L., Williams, C.K.I., Winn, J., Zisserman, A., 2010. The pascal visual object classes (voc) challenge. Int. J. Comput. vis. 88 (2), 303–338.

Farnell, D.J.J., Hatfield, F.N., Knox, P., Reakes, M., Spencer, S., Parry, D., Harding, S.P., 2008. Enhancement of blood vessels in digital fundus photographs via the application of multiscale line operators. J. Franklin Inst. 345 (7), 748–765.

Ferris, F.L., 1993. How effective are treatments for diabetic retinopathy? JAMA 269 (10), 1290–1291.

Figueiredo, I.N., Kumar, S., Oliveira, C.M., Ramos, J.a.D., Engquist, B., 2015. Automated lesion detectors in retinal fundus images. Comput. Biol. Med. 66, 47–65.

Fleming, A.D., Philip, S., Goatman, K.A., Olson, J.A., Sharp, P.F., 2006. Automated microaneurysm detection using local contrast normalization and local vessel detection. IEEE Trans. Med. Imag. 25 (9), 1223–1232.

Fraz, M.M., Badar, M., Malik, A.W., Barman, S.A., 2018. Computational methods for exudates detection and macular edema estimation in retinal images: a survey. Arch. Comput. Method. Eng. 1–28.

Fu, H., Cheng, J., Xu, Y., Wong, D.W.K., Liu, J., Cao, X., 2018. Joint optic disc and cup segmentation based on multi-label deep network and polar transformation. arXiv preprint arXiv:1801.00926.

Fu, H., Xu, Y., Wong, D.W.K., Liu, J., 2016. Retinal vessel segmentation via deep learning network and fully-connected conditional random fields. In: Biomedical Imaging (ISBI), 2016 IEEE 13th International Symposium on. IEEE, pp. 698–701.

García, G., Gallardo, J., Mauricio, A., López, J., Del Carpio, C., 2017. Detection of diabetic retinopathy based on a convolutional neural network using retinal fundus images. In: International Conference on Artificial Neural Networks. Springer, pp. 635–642.

Garcia, M., Sanchez, C.I., Poza, J., López, M.I., Hornero, R., 2009. Detection of hard exudates in retinal images using a radial basis function classifier. Annal. Biomed. Eng. 37 (7), 1448–1463.

Gargeya, R., Leng, T., 2017. Automated identification of diabetic retinopathy using deep learning. Ophthalmology 124 (7), 962–969.

Gegundez-Arias, M.E., Marin, D., Bravo, J.M., Suero, A., 2013. Locating the fovea center position in digital fundus images using thresholding and feature extraction techniques. Comput. Med. Imag. Graph. 37 (5–6), 386–393.

Giachetti, A., Ballerini, L., Trucco, E., 2014. Accurate and reliable segmentation of the optic disc in digital fundus images. J. Med. Imag. 1 (2), 024001.

Giancardo, L., Meriaudeau, F., Karnowski, T.P., Li, Y., Garg, S., Tobin, K.W., Chaum, E., 2012. Exudate-based diabetic macular edema detection in fundus images using publicly available datasets. Med. Image Anal. 16 (1), 216–226.

Giancardo, L., Meriaudeau, F., Karnowski, T.P., Li, Y., Tobin, K.W., Chaum, E., 2011. Microaneurysm detection with radon transform-based classification on retina images. In: 2011 Annual International Conference of the IEEE Engineering in Medicine and Biology Society. IEEE, pp. 5939–5942.

Giancardo, L., Roberts, K., Zhao, Z., 2017. Representation learning for retinal vasculature embeddings. In: Fetal, Infant and Ophthalmic Medical Image Analysis. Springer, pp. 243–250.

Glorot, X., Bengio, Y., 2010. Understanding the difficulty of training deep feedforward neural networks. In: Proceedings of the Thirteenth International Conference on Artificial Intelligence and Statistics, pp. 249–256.

Greenspan, H., Van Ginneken, B., Summers, R.M., 2016. Guest editorial deep learning in medical imaging: overview and future promise of an exciting new technique. IEEE Trans. Med. Imag. 35 (5), 1153–1159.

van Grinsven, M.J., van Ginneken, B., Hoyng, C.B., Theelen, T., Sánchez, C.I., 2016. Fast convolutional neural network training using selective data sampling: application to hemorrhage detection in color fundus images. IEEE Trans. Med. Imag. 35 (5), 1273–1284.

Gu, J., Wang, Z., Kuen, J., Ma, L., Shahroudy, A., Shuai, B., Liu, T., Wang, X., Wang, G., Cai, J., et al., 2018. Recent advances in convolutional neural networks. Pattern Recognit. 77, 354–377.